Stress-Driven Phase Transformation and the Roughening of Solid-Solid Interfaces

L. Angheluta, E. Jettestuen, J. Mathiesen, F. Renard, B. Jamtveit

HAL Id: insu-00331988
https://insu.hal.science/insu-00331988

Submitted on 12 Jan 2009

Stress-driven phase transformation and the roughening of solid-solid interfaces

L. Angheluta[1], E. Jettestuen [1], J. Mathiesen[1], F. Renard[1,2], B. Jamtveit[1]

[1] *Physics of Geological Processes, University of Oslo, Oslo, Norway*

[2] *LGCA-CNRS-OSUG, University of Grenoble, BP 53, F-38041, France*

(Dated: January 13, 2008)

The application of stress to multiphase solid-liquid systems often results in morphological instabilities. Here we propose a solid-solid phase transformation model for roughening instability in the interface between two porous materials with different porosities under normal compression stresses. This instability is triggered by a finite jump in the free energy density across the interface, and it leads to the formation of finger-like structures aligned with the principal direction of compaction. The model is proposed as an explanation for the roughening of stylolites - irregular interfaces associated with the compaction of sedimentary rocks that fluctuate about a plane perpendicular to the principal direction of compaction.

Morphological instabilities in systems out of equilibrium are central to most research on pattern formation. A host of processes give rise to such instabilities, and among the most intensively studied are the surface diffusion mediated Asaro-Tiller-Grinfeld instability [1–3] in the surfaces of stressed solids in contact with their melts, surface diffusion mediated thermal grooving and solidification controlled by thermal diffusion in the bulk melt [4]. In sedimentary rocks and other porous materials local stress variations typically promote morphological changes via dissolution in regions of high stress, transport through the fluid saturated pore space and precipitation in regions of low stress. This phenomenon is known as pressure solution or chemical compaction. Such processes are often accompanied by the nucleation and growth of thin irregular sheets, interfaces or seams called stylolites [5]. Stylolites form under a wide range of geological conditions as rough interfaces that fluctuate about a plane perpendicular to the axis of compression. They are common in a variety of rock types, including limestones, dolomites, sandstones and marbles, and they appear on scales ranging from the mineral grain scale to meters or greater. A common feature of stylolitic surfaces is small scale roughness combined with large vertical steps in the direction of the compression. Residual unsoluble minerals (i.e. clays, oxides) often accumulate at the interface as stylolites evolve. Despite the considerable attention given to the rich morphology of stylolites there is still no consensus on the mechanism(s) controlling their formation [6–9]. Here we demonstrate that even if the stylolite is a consequence of pressure solution alone, porosity or other material property gradients may drive the roughening process. In particular, we demonstrate that a compressional load normal to a no-slip solid-solid phase boundary gives rise to a morphological instability. Our setup differs from the commonly studied solid-melt systems, where stresses are applied in the lateral direction and the melt is in a hydrostatic state (see e.g. [10]).

Generally, rocks are heterogeneous bodies with spatially variable porosities. The strain energy densities may be larger in regions of high porosity (i.e. low modulus) than in regions of low porosity. Thermodynamically, the total free energy of the system can be reduced by decreasing the porosity variations. In this letter, a simple model for stylolite formation, in which high porosity rock is transformed into low porosity rock at the interface between the low porosity and high porosity materials, is investigated. This solid-solid "phase transformation" is driven by gradients in the free energy per unit volume of mineral, which can be substantial in regions with large porosity variations. The general approach used in this work could be applied to other solid-solid interface roughening phenomena.

We consider a two-dimensional system divided into elastic regions with different but homogeneous porosities (Fig. 1). Without lack of generality, we limit our consideration to two dissimilar materials separated by a single interface. The stress boundary condition is a uniform compression in the vertical direction applied at the top and bottom boundaries. The two phases are separated by a sharp and coherent boundary, i.e. no defects or voids can form along the interface. This translates into continuity of the displacement vector $\mathbf{u}(\mathbf{r}, t)$ across the interface, $[\mathbf{u}] = 0$. Here, and in other equations the brackets denote the jump in the quantity inside the brackets when the interface is approached from above and below. Under given load conditions the displacement field induced by the compression gives rise, in the linear regime, to a strain tensor of the form

$$\epsilon_{ij} = \frac{1}{2}\left(\frac{\partial u_j}{\partial x_i} + \frac{\partial u_i}{\partial x_j}\right). \tag{1}$$

The two solid phases are characterized by their Young's moduli, $E_{1,2}$, and Poisson's ratios, $\nu_{1,2}$. When $E_1 < E_2$, the upper region will be compressed the most and therefore the elastic energy density will be higher in this region. The first step towards a model for the roughening of a solid-solid interface is based on this simple observation. First the elastic parameters of the materials are
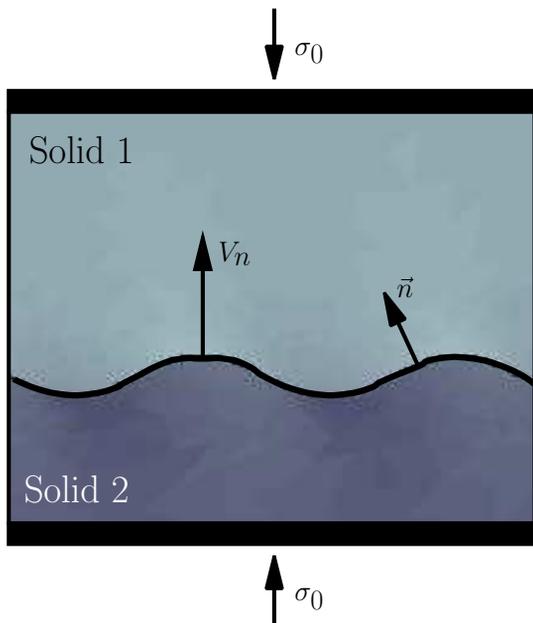
FIG. 1: (Color online) Basic setup of the model for a moving interface between two elastic solid phases, characterized by different Young's moduli ($E_2 > E_1$) and Poisson's ratios ν_1, ν_2. The interface boundary propagates with a normal velocity V_n, when the solids are subjected to uniform far-field compressional stresses σ_0 in the vertical direction.

related to their porosities. Luo and Weng [11] proposed a homogenization method relating the effective bulk and shear moduli to the porosity of the solid. Using this approach, the effective Young's modulus decreases monotonically with the porosity. Consequently, a finite jump in porosity across the interface induces a jump in the elastic energy density, which drives the motion of the interface. Thermodynamically, the evolution of the interface corresponds to a phase transformation from a high to a low energy state.

It is assumed that the phase transformation occurs on a time scale that is much longer that the time required for elastic waves to propagate across the system, and the system is therefore always in elastostatic equilibrium. For an isotropic and homogeneous elastic body the elastic equilibrium condition is given by

$$\frac{\partial \sigma_{ij}}{\partial x_j} = 0, \qquad (2)$$

together with the uniform uniaxial compression stress boundary condition, $\sigma_{ij}(x, y = \infty) = \sigma_0 \delta_{i,y} \delta_{j,y} < 0$, and the stress jump across the curved interface due to the effective surface tension is given by

$$[\sigma_{ij} n_j] = -\gamma \kappa n_i \text{ at the interface } \Gamma_t, \qquad (3)$$

where κ is the curvature and γ is the local surface tension. In the limit of negligible surface tension, the stress vector is continuous across the interface ($[\sigma_{ij} n_j] = 0$).

For completeness, the basic principles used to derive an equation of motion are presented. When the system approaches an equilibrium configuration, the free energy will be a non-increasing function of time:

$$\frac{d}{dt}\left(\int_V \mathcal{F} dv + \int_{\Gamma_t} \tilde{\mathcal{F}} ds \right) \leq 0, \qquad (4)$$

where $\mathcal{F}$ is the free energy per unit volume and $\tilde{\mathcal{F}}$ is the interfacial free energy per unit area. Here, the subscript V indicates a volume integration and Γ_t indicates integration over the interface. The interfacial energy dissipation is obtained by confining the domain of integration to a narrow zone along the interface and taking the zero thickness limit [12]. This gives

$$-\int_{\Gamma_t} [\mathcal{F}] V_n ds + \int_{\Gamma_t} \left(\frac{d\tilde{\mathcal{F}}}{dt} - \kappa \tilde{\mathcal{F}} V_n \right) ds \leq 0, \qquad (5)$$

where V_n is the normal velocity and κ is the local curvature of the interface. This implies the differential form given by

$$\frac{d\tilde{\mathcal{F}}}{dt} - (\kappa \tilde{\mathcal{F}} + [\mathcal{F}]) V_n \leq 0, \qquad (6)$$

where the first term is the total time derivative of the local interfacial energy density. The local free energy is a function of the surface tension only (like fluid-solid interfaces) and thus, it is independent of time. Therefore, the time derivative can be neglected leading to the inequality

$$-(\kappa \tilde{\mathcal{F}} + [\mathcal{F}]) V_n \leq 0. \qquad (7)$$

In the linear response regime, this inequality is satisfied when the velocity (the thermodynamic flux) is a linear function of the driving force, $(\kappa \tilde{\mathcal{F}} + [\mathcal{F}])$, namely

$$V_n \sim c\left(\kappa \tilde{\mathcal{F}} + [\mathcal{F}] \right), \qquad (8)$$

with $c \geq 0$. In the absence of surface tension, the normal velocity is simply proportional to the jump in the strain energy, i.e. $V_n \sim [\mathcal{F}]$. While the dynamical law for the interface Eq. (8) is very simple, the implementation in a numerical model is more challenging.

The model (Fig. 1) of the moving solid-solid interface was numerically implemented using the local force balance and energy dissipation equations (Eqs. (3) and (8)). The stress field is obtained using the Galerkin finite element discretization of the elastostatic equations and the phase boundary is captured using the level set method. The level set method ([13]) is a powerful and reliable technique for tracking surfaces in any number of dimensions. At any time t, the d-dimensional interface Γ_t may be defined as the zero level cut through a scalar field φ (d+1-dimensional surface), namely, $\varphi(\mathbf{x}, t) = 0$, where $\mathbf{x} \in \Gamma_t$. A change in the zero-level cut in response to a change in
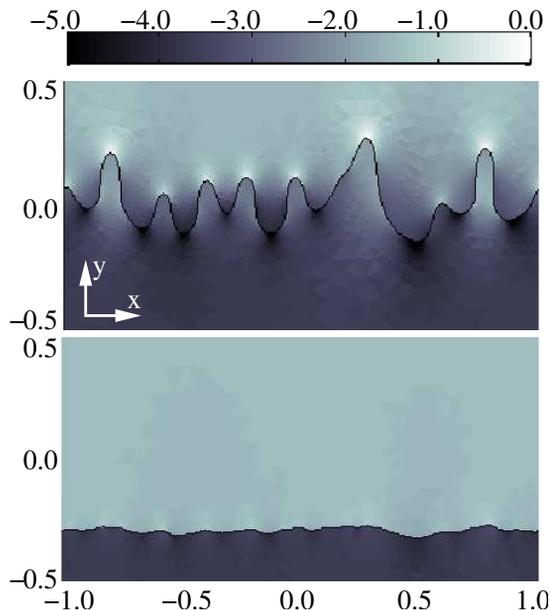
FIG. 2: (Color online) Map of the logarithm of the elastic energy in the solids during the roughening process, with $E_1 = 10$ GPa, $E_2 = 60$ GPa, $\nu_1 = \nu_2 = 0.3$, and $\sigma_0 = 0.05$ MPa. Lower panel: initial $h(x)$ at $t = 0$. Upper panel: interface at a later stage of roughening.
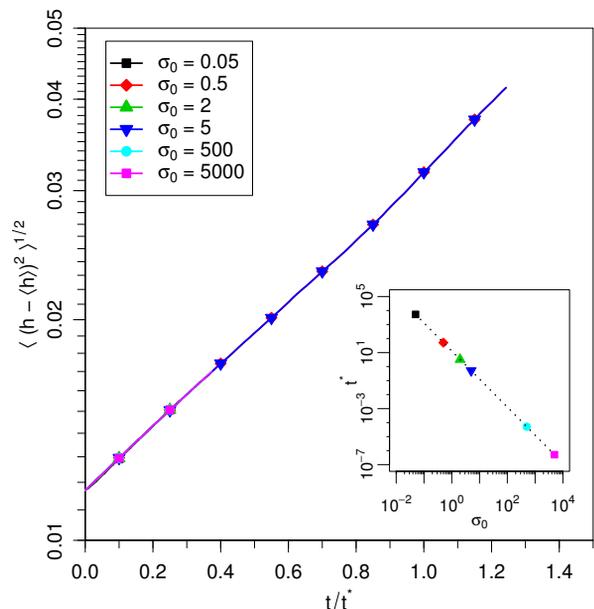

FIG. 3: (Color online) Roughness as a function of time for six different external compression stresses σ_0 (in units of 10^5 Pa, see legend) for a fixed jump in the Young's modulus and zero surface tension. The root means square height is plotted as a function of time, rescaled with the characteristic roughening time t^*, on a semi-logarithmic scale. The data collapse shows the exponential roughening of the interface $\exp(t/t^*)$ with a stress independent pre-exponential factor. Inset: the characteristic time as a function of σ_0 is given by $t^* \sim \sigma_0^{-2}$ (shown by the dashed line).

the scalar field may then be interpreted as a motion of the interface. Therefore the change in the scalar field must correspond to motion of the zero-level cut with a given normal velocity $\mathbf{V}$, this is done by updating the scalar field using a simple advection-like equation

$$\frac{\partial \varphi}{\partial t} + V_{\mathrm{n}} |\nabla \varphi| = 0. \qquad (9)$$

The advection of the level set function is solved on a separate lattice using an upwind-scheme. The full dynamical model of the solid-solid phase transformation front is then given by this equation together with Eq. (8).

In the numerical simulations, we have used periodic boundary conditions in the lateral direction to reduce possible finite size effects. The initial interface was generated by a directed random walk (Fig. 2, lower panel). The temporal evolution of the interface (Fig. 2, upper panel) was then recorded for different external stresses, σ_0, and elastic constants (E, ν). The elastic constants were computed from homogenization relations between elasticity and porosity [11]. As the interface advances increasing lateral stresses may appear behind the tips of the finger like structures. While such lateral stress may cause interface instability, it will only have a secondary effect on the overall transversal evolution.

Initially, the roughness of the interface grows exponentially

$$\sqrt{\int_{\Gamma_t} \left(h(s,t) - \overline{h}(t) \right)^2 ds} \sim \exp(t/t^*), \qquad (10)$$

with a characteristic roughening time t^* that depends on the external stress and the jump in the elastic properties. To estimate the functional dependence of t^*, a set of numerical simulations was performed. First, the external stress σ_0 was systematically varied between 0.005 and 500 MPa for fixed values of the elastic constants ($E_1 = 40$ GPa, $E_2 = 60$ GPa, $\nu_1 = \nu_2 = 0.3$).

The results shown in Fig. 3 suggests that the characteristic time scales as $t^* \sim \sigma_0^{-2}$, and the prefactor depends on the elastic properties. In order to investigate this type of relation, the elastic constants across the interface were varied ($E_2 = 50$ GPa, E_1 in the range 5-16 GPa, $\nu_1 = \nu_2 = 0.3$). The data for the interface roughening collapses onto a curve which is exponential at small time-scales with a cross-over to a quadratic form at larger times (Fig. 4). Extracting the characteristic time in the exponential growth regime and rescaling it with σ_0^2, the functional dependence with respect to the jump in the elastic constants across the interface was determined (see Fig. 4, inset). The cross-over from exponential to algebraic roughening depends on the value of the jump. For large jumps in the elastic energy or porosity, the roughening quickly undergoes a transition from exponential to quadratic growth in time. This cross-over time is related to the formation and growth of the finger-like structures
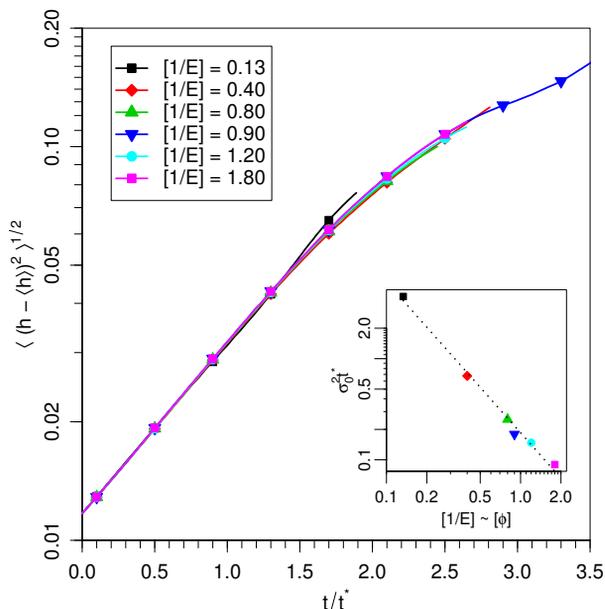
FIG. 4: (Color online) Roughness as a function of time for different jumps in the Young's modulus $[1/E] = 1/E_1 - 1/E_2$ (measured in units of 10^{-10}Pa, see legend) for fixed external stress ($\sigma_0 = 5$MPa) and zero surface tension. The data is plotted against the time rescaled with t^* estimated numerically from the initial exponential growth. At large times, the roughness grows quadratically with increasing time. Inset: Log-log plot of the characteristic time rescaled with the corresponding external stress $\sigma_0^2 \cdot t^*$ as a function of the jump $[1/E]$. $t^* \sim \sigma_0^2 \cdot [1/E]^{-\alpha}$. As guide to the eye, we added a dashed line with exponent $\alpha = 3/2$.

due to transport of dissolved minerals and precipitation leading to pore clogging. Stress concentration at the tips is an important characteristic of the system and the pronounced contrast in the energy density between the two phases leads to an enhanced chemical activity. In stylolites the roughening is often accompanied by small fractures aligned with the direction of compression, and this may be explained by the model if the stress concentration at the fingers exceeds the yield strength of the material.

To summarize, a simple solid-solid phase transformation model that predicts a morphological instability of the interface under uniform compressional stress has been developed and investigated. The instability is triggered by a finite jump in the elastic properties across the interface and a concomitant jump in the free energy density. We also showed that the characteristic time of roughening depends on the external applied stress and the elastic parameters jump, in such a way that a higher external compression load or a larger difference between the elastic properties of the phases shortens the time required to roughen the interface. This result allows the roughening time and formation rate of stylolites to be estimated as a function of burial depth in sedimentary basins.

shown in Fig. 2. By a simple dimensional argument, we also determined that the generic dependence of t^* on the external stress and elastic constants, has the form

$$t^* \sim \frac{L}{V_n} \sim \frac{L}{c[\mathcal{F}]} \sim \frac{L}{c} \frac{1}{[(1-\nu^2)/E]} \frac{1}{\sigma_0^2}, \qquad (11)$$

where $[\mathcal{F}] = \mathcal{F}_1 - \mathcal{F}_2$ is the jump in the free energy density across the interface. The scaling relation is consistent with the numerical simulation results. The stress field may be calculated analytically with the same boundary and interface conditions for a straight interface perturbed by a sine function with small amplitude A. In linear perturbative analysis ($A \ll 1$) without surface tension, the solution is obtained using the method of Airy's potentials for 2D elastostatics [14]. The energy jump $[E]$ is proportional to kA^2, where $k = 2\pi/\lambda$ is the wave number. In other words, all the modes are unstable and those with the smaller wavelengths grow faster in the linear regime. The surface tension adds an ultraviolet cut-off resulting in small scales smoothening of the interface. The system was tested with and without surface tension and in both cases the qualitative behavior was the same - an initial exponential roughening with a crossover to a finger-formation regime. Eventually, these fingers may stabilize

[1] R. J. Asaro and W.A. Tiller, Metallurgical Transactions **3**, 1789 (1972).

[2] M. A. Grinfeld, Dolk. Akad. Nauk SSSR **290**, 1358 (1986).

[3] D. J. Srolovitz, Acta Metall. **37** 2, 621 (1989).

[4] W. Mullins, Journal of Applied Physics **28** 3, (1957)

[5] P. B. Stockdale, Indiana University Studies, **IX**, 1 (1922); M. T. Heald, Journal of Geology, **63**, 101 (1955); P. K. Weyl, Journal of Geophysical Research **64**, 11 (1959); W. Park and E. Schot, J. Sediment. Petrol. **38**, 175 (1968); R. Bathurst, *Carbonate sediments and their diagenesis*, Elsevier Science (1971).

[6] E. H. Oelkers and P.A. Bjørkum and W.M. Murphy, American Journal of Science **296**, 420 (1996).

[7] J. Schmittbuhl and F. Renard and J. P. Gratier and R. Toussaint, Phys. Rev. Lett. **93**, 238501 (2004).

[8] E. Aharonov and R. Katsman, "Modeling stylolite formation", preprint

[9] D. Koehn and F. Renard and R. Toussaint and C. W. Passchier, Earth Planet. Sci. Lett. **257**, 582 (2007).

[10] Y. Xiang and W. E, J. Appl. Phys. **91**, 9414 (2002).

[11] H. A. Luo and G. J. Weng, Mech. Materials **6**, 347 (1987).

[12] M. E. Gurtin, Journal of Applied Mathematics and Physics (ZAMP) **42**, (1991).

[13] J. A. Sethian, *Level Set Methods and Fast Marching Methods*, Cambridge, 2nd Ed. (1999); S. Osher, and R. Fedkiw, *Level Set Methods and Dynamic Implicit Surfaces*, Springer (2003).

[14] H. Gao, Int. J. Solids Structures, **28**, 703 (1991).